Free-energy calculations of intrinsic point defects in silicon

O. K. Al-Mushadani* and R. J. Needs
TCM Group, Cavendish Laboratory, University of Cambridge, Madingley Road, Cambridge CB3 0HE, United Kingdom
(Received 21 July 2003; published 5 December 2003)

We study the energetics of various point defects in silicon using *ab initio* density-functional methods. The formation free energies are calculated from the harmonic phonon frequencies, which are determined from *ab initio* density-functional perturbation theory calculations. We deduce the concentrations of defects as a function of temperature and compare them with experimental estimates. The localized vibrational modes associated with the various defects are described.

DOI: 10.1103/PhysRevB.68.235205 PACS number(s): 61.72.Ji, 63.20.Mt, 71.55.Cn

I. INTRODUCTION

Intrinsic point defects in silicon have attracted a great deal of interest because of the technological importance of the material. In particular they strongly influence the diffusion of dopant atoms at elevated temperatures during device manufacture. Both experimental and theoretical techniques have been brought to bear on these defects but fundamental gaps in our understanding still exist. Unfortunately it has not been possible to detect silicon self-interstitials directly and we must rely on theoretical techniques to elucidate their microscopic nature. In the case of neutral vacancies, electron-paramagnetic-resonance studies[1] have determined unambiguously their symmetry to be D_{2d}, which is consistent with a Jahn-Teller distortion. Positron-lifetime experiments give a value for the enthalpy of formation of a neutral vacancy in silicon of 3.6 ± 0.2 eV.[2]

The self-diffusivity can be measured at high temperatures using radioactive isotopes as tracers, and experimental estimates of the contributions to the self-diffusivity from self-interstitials and vacancies have been made.[3,4] The self-diffusivity D_{SD} can be written as the sum of contributions from independent mechanisms, $D_{\mathrm{SD}}=\Sigma_j f_j D_j n_{d,j}$, where f_j are correlation factors of order unity, D_j is the diffusivity, and $n_{d,j}$ is the concentration of defect j. The situation regarding the separate values of D_j and $n_{d,j}$ for vacancy and self-interstitial mechanisms is very unclear, with estimates differing wildly.[5] This gap in our knowledge is important because one requires D_j and $n_{d,j}$ separately to predict the behavior for nonequilibrium defect concentrations, which occur during the processing of silicon.

In this contribution we calculate the formation free energies of intrinsic point defects in silicon, including the vibrational contributions, using *ab initio* density-functional theory (DFT) methods. From these we deduce the equilibrium concentration of defects as a function of temperature. We have studied the neutral vacancy, the hexagonal, and split$\langle 110 \rangle$ self-interstitials, and the fourfold-coordinated defect (FFCD). The FFCD has not been detected experimentally, but *ab initio* calculations indicate that it has the lowest formation energy of any intrinsic point defect in silicon,[6] and therefore its properties are of interest. We also study the localized vibrational modes associated with the defects.

II. EQUILIBRIUM DEFECT CONCENTRATION

The total free energy of a solid F_{tot} can be approximated as the sum of the internal energy at zero temperature E and the vibrational free energy F_{vib}

$$F_{tot}=E+F_{vib}. \tag{1}$$

The change in free energy on introducing a single point defect is

$$\Delta F^{defect}=F_{tot}^{defect}-\frac{N+\{-1,0,1\}}{N}F_{tot}^{bulk}, \tag{2}$$

where N is the number of atoms in the perfect crystal and the quantity in braces takes the value $+1$ for an interstitial, 0 for the FFCD, and -1 for the vacancy. Adding the term from the configurational entropy of the defect gives the total formation free energy,

$$\Delta F^{solid}=n_d \Delta F^{defect}-TS_{conf}[n_d], \tag{3}$$

where there are n_d defects per unit volume. Each defect has n_i degenerate configurations per lattice site, and the total number of atoms per unit volume is n_s. The configurational entropy per unit volume is therefore given by

$$S_{conf}=-k_B \ln\left[\frac{n_s!}{(n_s-n_d)!\,n_d!}n_i^{n_d}\right]. \tag{4}$$

Minimizing ΔF^{solid} with respect to n_d and assuming $n_d \ll n_s n_i$ gives the equilibrium concentration of defects,

$$n_d^*=n_s n_i \exp\left[-\frac{\Delta F}{k_B T}\right]. \tag{5}$$

III. METHOD

We have performed zero-temperature calculations of the relaxed structures and formation energies of the defects using DFT methods within the local-density approximation[7] (LDA). We then use density-functional perturbation theory (DFPT) (Ref. 8) to obtain phonon spectra of the defective and perfect crystals from which we deduce the vibrational free energy. We have adopted a plane-wave pseudopotential framework and all calculations were performed using the ABINIT code.[9] The defects were contained within 64-atom simple cubic supercells subject to periodic boundary condi-

TABLE I. Formation energies of the defects.

	Formation energy (eV)
Vacancy	3.53
Hexagonal	3.45
Split⟨110⟩	3.40
FFCD	2.80
Displaced hexagonal	3.42

tions. A plane-wave cutoff energy of 12 hartree was used for all calculations, which provides good convergence for both the electronic and vibrational contributions to the free energies. We used a Troullier-Martins[10] LDA pseudopotential to represent the Si^{4+} ions. Unless otherwise stated, we used the relaxed LDA cubic lattice constant of 5.387 Å, which is a little smaller than the experimental value of 5.429 Å. The Brillouin-zone integrations were performed using the Monkhorst-Pack[11] sampling scheme with a $3\times3\times3$ grid of **k** points.

The ground-state structures of the defects were obtained by relaxing the structures until the Hellmann-Feynman[12] forces on the atoms were less than 5×10^{-6} eV/Å, which is an extremely fine tolerance. Small, random displacements were applied to the atoms before relaxation to remove any initial symmetry which could otherwise be locked in. The forces were calculated using the same energy cutoffs and **k**-point grids throughout. It has recently been reported[13] that this is important to ensure the correct relaxation of atoms which may otherwise end up in a higher-energy local minimum.

Various studies[6,13,14] have indicated that large supercells are required to obtain full convergence of the formation energies, and even then the agreement between the different studies is not particularly good, with estimates of the defect formation energies differing by several tenths of an eV. In our tests we found that the formation energy of the FFCD in a 54-atom face-centered cubic supercell differed from that obtained with a 64-atom simple cubic cell by about 0.2 eV.

The formation energies of the various defects are given in Table I. These results show that the FFCD has the lowest formation energy. The FFCD was recently studied using *ab initio* DFT methods by Goedecker *et al.*,[6] although in fact it corresponds to the interstitial-vacancy defect found in earlier tight-binding calculations.[15,16] This defect is low in energy because it maintains the fourfold coordination of the bulk crystal. The hexagonal and split⟨110⟩ interstitials are essentially degenerate in energy as found in previous studies.[6,17,18] The vacancy has a higher formation energy than the self-interstitials within the LDA, in agreement with most recent results.[6,19] We have found the hexagonal interstitial to have an unstable phonon mode, and on following the displacement along the corresponding eigenvector we located a stable structure with a formation energy 0.03 eV lower than the hexagonal interstitial. The displaced hexagonal defect is derived from the hexagonal defect by a displacement of the interstitial atom, shown in black in Fig. 2, out of the hexagonal ring by 0.48 Å.

Even after the technical issues of plane-wave cutoff, **k**-point sampling and supercell size have been resolved, the relative energies of the defects are still sensitive to the treatment of the electronic correlation. Studies[6,17,20] using the generalized gradient approximation (GGA) to DFT give a different energy ordering of the candidate defects. The GGA formation energies for the interstitial defects are larger than the LDA ones while the vacancy formation energy is lower, so that within the GGA the interstitial defects have the highest formation energies. The FFCD remains lower in energy than the other defects. A diffusion quantum Monte Carlo study[21] by Leung *et al.*[20] gave even larger interstitial defect formation energies.

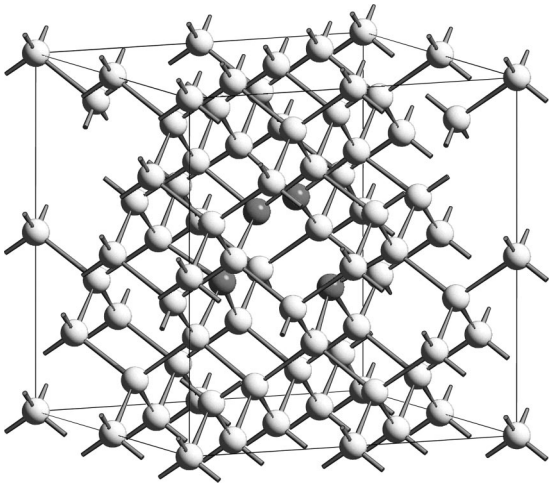

FIG. 1. Neutral vacancy defect. The first-nearest-neighbor atoms to the vacancy are shown in dark gray.

IV. DEFECT STRUCTURES

Figures 1–4, produced using the SCHAKAL[22] package, show the relaxed structures of the various defects. The number of degenerate configurations n_i of each defect per lattice site can be determined from the symmetries of the structures

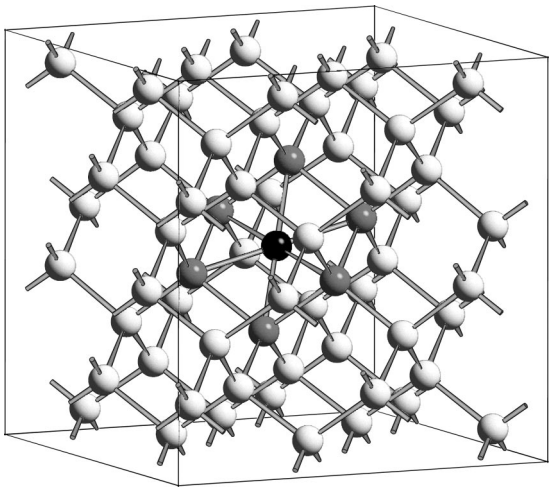

FIG. 2. Hexagonal interstitial defect. The interstitial atom is shown in black. The first-nearest-neighbor atoms are shown in dark gray.

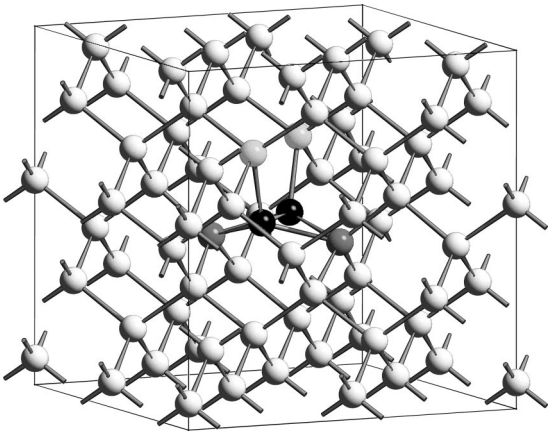

FIG. 3. Split$\langle 110\rangle$ interstitial defect. The interstitial pair of atoms are shown in black, the first nearest neighbors are in dark gray and second nearest neighbors are in light gray.

and is given in Table III. This information is needed to obtain the total defect concentrations using Eq. (5).

The silicon vacancy probably poses the greatest difficulty for *ab initio* studies of defects. Previous calculations have shown the energy surface near the minimum to be quite shallow. This has meant that various studies have found different minimum energy structures. Some dedicated expositions[13,14,23,24] have shown how the defect structure is dependent on convergence parameters and how the atomic relaxation is carried out. The experimental picture is much more conclusive. Electron-paramagnetic-resonance studies[1] have shown that the vacancy has D_{2d} symmetry. The studies mentioned above also conclude that this is the case when large supercells and adequate **k**-point grids are used. The present study also gives a structure which has D_{2d} symmetry. The bond distances between the four ions neighboring the vacancy, shown in dark gray in Fig. 1, are given in Table II. We see that these atoms form two pairs with bond lengths of 3.415 Å. The four bond lengths between different pairs are slightly longer at 3.425 Å. This is in accordance with previous findings for a D_{2d} structure having two bonds of one length and four of another. The present results are, however, close to T_d symmetry as the two distinct distances are closer in our study than in previous ones. A true T_d structure would have six identical bond lengths. The number of degenerate states of the D_{2d} symmetry defect is $n_i=3$, corresponding to the number of independent ways of choosing two pairs from four atoms.

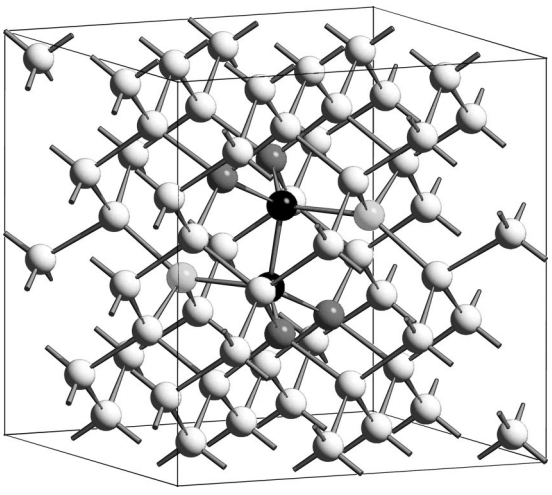

FIG. 4. The FFCD. The interstitial pair of atoms is shown in black, the first nearest neighbors are in dark gray and second nearest neighbors are in light gray.

TABLE II. Bond lengths between the four atoms neighboring the vacancy.

	1	2	3	4	5	6
Distances (Å)	3.415	3.415	3.425	3.425	3.425	3.425

For the hexagonal interstitial we found a bond length of 2.361 Å between the interstitial and each of its six nearest neighbors, which is close to a previous result[17] of 2.360 Å. If the symmetry is perfectly hexagonal we have $n_i=2$ for this defect. This result disagrees with that in a previous paper,[25] which we believe to be incorrect. The displaced hexagonal defect has $n_i=4$.

The split$\langle 110\rangle$ defect consists of a pair of atoms sharing an atomic site of the perfect crystal. The pair, shown in black in Fig. 3, are aligned along a $\langle 110\rangle$ zigzag chain. The bond length between the defect pair of 2.432 Å is slightly larger than the bulk bond length of 2.333 Å, and is very similar to the value of 2.44 Å found in an earlier study.[17] The pair of atoms forming the split$\langle 110\rangle$ defect are both fourfold coordinated. The neighboring atoms, colored dark gray in Fig. 3, are fivefold coordinated and their bonds to the defect pair are 2.455 Å long, which is close to the value of 2.46 Å found in a previous study.[26] The bond distance between the defect pair and the light gray atoms in the zigzag chain is, however, shorter than the bulk bond length at 2.315 Å. For this defect the number of degenerate states is $n_i=6$, which corresponds to the number of ways of choosing two bond directions from four.

The FFCD defect consists of a pair of atoms, shown in black in Fig. 4, that have been rotated from their normal positions within the bulk crystal. The present calculations give the bond length between the two defect atoms as 2.227 Å, which is close to the value of 2.25 Å found in a GGA-DFT study.[6] The other three bonds formed by the defect atoms are longer. There are a pair of length 2.346 Å from the black to the dark gray atoms and one of length 2.457 Å to the light gray atom. The FFCD has $n_i=6$.

V. PHONON CALCULATIONS

We calculated the phonon spectra of the same supercells used in the ground state electronic structure calculations within linear-response theory using *ab initio* DFT. For consistency we used the same **k**-point grids, pseudopotential, and plane-wave cutoffs as before. We calculated the dynamical matrix at the Γ point of the supercell, which was Fourier transformed into real space to give the matrix of interatomic force constants. This was then Fourier transformed back into momentum space to obtain interpolated dynamical matrices

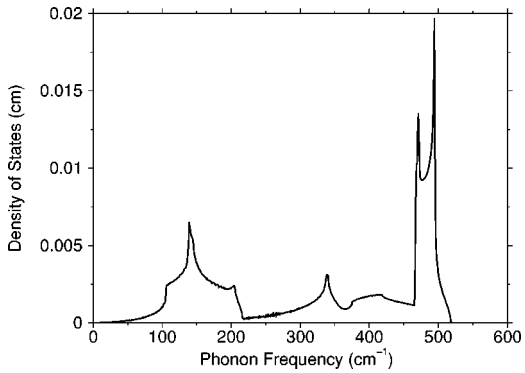

FIG. 5. Phonon density of states of bulk silicon.

at any point in the Brillouin zone. Diagonalization of the dynamical matrices yields the phonon frequencies and corresponding eigenvectors. The responses need only be calculated at the Γ point for the defect structures as the large size of the supercells guarantees convergence of the phonon spectrum. Test calculations on a smaller 54-atom face-centered cubic supercell showed that the 64-atom supercell is adequate for calculations of defect phonon spectra.

The calculated phonon densities of states for bulk silicon and the defective structures are shown in Figs. 5–10. The bulk density of states shows four main groups of phonons. The first group is located between 100 and 200 cm^{-1}. This lies just above the acoustic region in which the density of states increases roughly as ω^2. The second group has less weight and builds up slowly from a minimum just above 200 cm^{-1} to a peak at 340 cm^{-1}. The density of states then falls before building up to form the third group between 370 and 460 cm^{-1}. This group has roughly the same cumulative weight as the second one. Following this the density of states increases sharply at 460 cm^{-1} to form the last group which has considerable weight. This group finishes at roughly 520 cm^{-1} where the density of states falls to zero.

From Figs. 5 to 10 we see that the densities of states for the 64-atom supercells remain largely unchanged upon insertion of a single defect. One of the effects of introducing the defects is that the van Hove singularities observed in the bulk phonon density of states are smeared out. The densities of states also become more jagged upon introduction of a

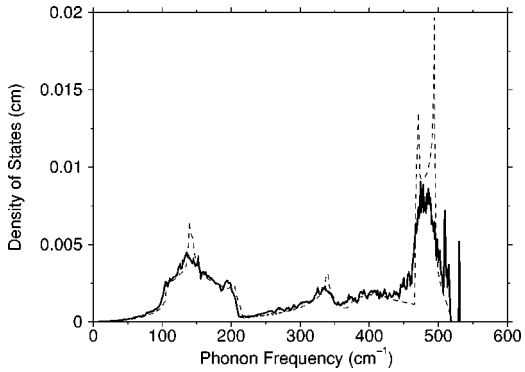

FIG. 6. Solid line: phonon density of states for a 64-atom supercell containing one FFCD, dashed line: bulk density of states.

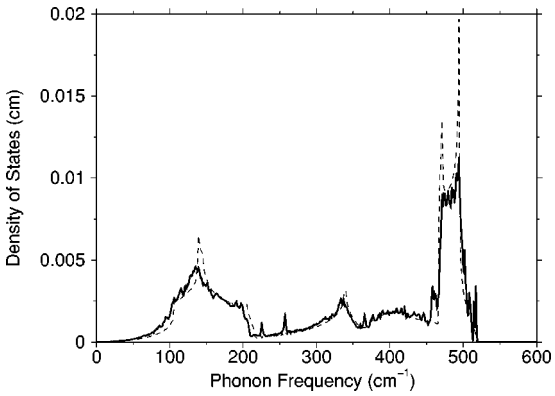

FIG. 7. Solid line: phonon density of states for a 64-atom supercell containing one split$\langle 110 \rangle$ defect, dashed line: bulk density of states.

defect as phonons which were degenerate in the bulk become nondegenerate. Of particular interest are the modes which appear above the highest calculated mode in the bulk, which are localized modes in which the associated normalized eigenvectors are dominated by motions of atoms close to the defect. Localized modes for point defects in silicon have been calculated before,[25] but these calculations used an empirical interatomic potential which gives the highest bulk phonon mode at 392 cm^{-1}, which is 24% lower than the experimental value. Our *ab initio* DFT results, however, give a much more accurate description of the entire phonon spectrum and it is possible to achieve deviations from experimental results of no more than a few inverse cm. An example of this is given by the agreement of the calculated optic mode frequencies at the Γ point at 517 cm^{-1} with the experimental[27] value of 518 ± 8 cm^{-1}. It is hoped that results for the defects will also be very accurate. This should be qualified, however, as the choice of lattice constant can have a significant effect on the phonon frequencies. If the experimental lattice constant of 5.429 Å is used then the highest phonon frequency is reduced by 2% to a value of 505 cm^{-1}. This error is still much smaller than in the empirical potential calculations, and since we are only interested in free-energy differences we may expect a certain

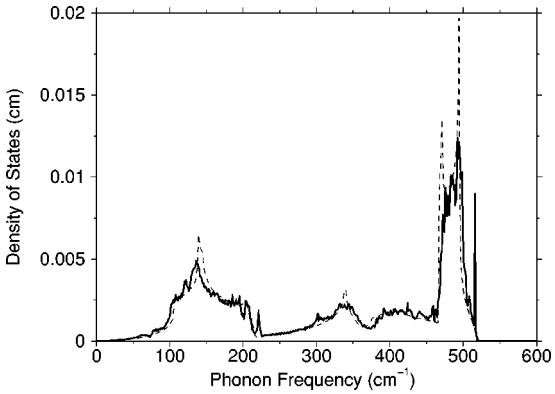

FIG. 8. Solid line: phonon density of states for a 64-atom supercell containing one hexagonal defect, dashed line: bulk density of states.

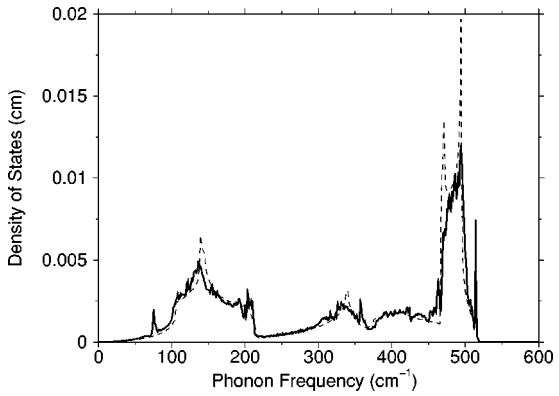

FIG. 9. Solid line: phonon density of states for a 64-atom supercell containing one displaced hexagonal defect, dashed line: bulk density of states.

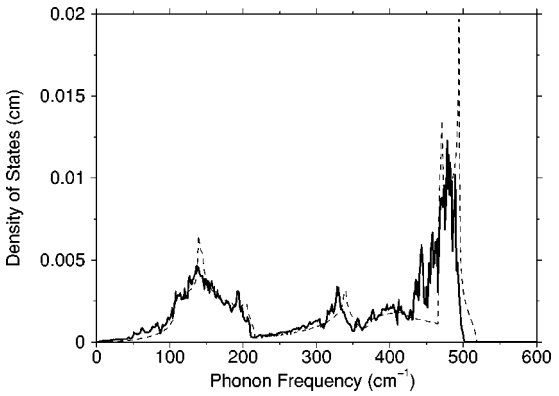

FIG. 10. Solid line: phonon density of states for a 64-atom supercell containing one vacancy, dashed line: bulk density of states.

amount of error cancellation. Tests showed that a cancellation of errors does tend to occur and ΔF depends only weakly on the choice of lattice constant, which also indicates that the effect of thermal expansion on ΔF is likely to be small.

Localized modes are characterized by large components of the normalized eigenvector being associated with atoms close to the defect. For the 64-atom bulk supercell the largest individual displacement is no greater than 0.215 compared to a value of 1.0 for a completely localized vibration. Despite not involving the addition or removal of silicon atoms, the rearrangement of atoms in the FFCD does produce a mode above the bulk cutoff. The pair of rotated atoms forming the defect have large motions associated with the highest-frequency mode at 530 cm^{-1}. Each of the defect atoms has a displacement of 0.644 which is substantially above the maximum in the bulk crystal. The four next-nearest-neighbor atoms, shown in dark gray in Fig. 4, have the smaller displacements of 0.145. The displacements of the atoms falls off with distance from the defect in this localized mode, although the decrease is not monotonic. Apart from this high-energy mode there are also some resonant modes in the continuum of the density of states which have a localized character. There is one mode at 407 cm^{-1} which is localized on a pair of atoms 6.6 Å away from the defect pair. Another mode at 511 cm^{-1} seems to be localized on the atoms surrounding the defect pair, shown in light gray in Fig. 4.

The split$\langle 110 \rangle$ also has localized vibrational modes. The mode with the largest atomic displacement occurs at 255 cm^{-1} corresponding to small but sharp peak in the phonon spectrum of Fig. 7. This resonant mode is centered on the two atoms of the defect pair, shown in black in Fig. 3, with a displacement of 0.520 for each atom. There is another resonant mode at 220 cm^{-1} which may be seen as a small spike in the phonon spectrum in Fig. 7. The highest mode at 518 cm^{-1} is localized with large displacements of the two neighbors of the defect pair colored light gray in Fig. 3. This mode resides just above the maximum frequency of the bulk phonons.

The hexagonal defect has localized modes at 516 cm^{-1} that appear as a sharp spike in the phonon spectrum given in Fig. 8. These modes are strongly localized on the interstitial atom and the hexagonal ring of nearest neighbors as shown by the black and gray atoms respectively in Fig. 2. There is also a resonant mode at 222 cm^{-1} centered on the interstitial which gives a small peak in the density of states.

We found the hexagonal defect to be unstable with respect to a displacement of the interstitial atom perpendicular to the plane of the hexagonal ring of atoms surrounding it. A single imaginary phonon frequency persists across the whole Brillouin zone. The hexagonal defect is thus shown to be a saddle-point configuration on the energy surface. The corresponding eigenvector at the Γ point indicates the direction of the instability. We displaced the atoms along the direction of this eigenvector and located the minimum in the energy. Further structural relaxation at this point using the forces gives the displaced hexagonal defect. The displaced hexagonal defect has a low frequency resonant mode at 76 cm^{-1}, see Fig. 9, which is strongly localized on the displaced interstitial atom. The eigenvector corresponds to a motion out of the plane of the ring with a magnitude of 0.767, indicating a very strongly localized mode. There are other resonant modes at 201 and 324 cm^{-1} associated with large vibrations of the neighboring atoms in the hexagonal ring. These modes do not, however, produce such a sharp spike in the density of states. There is a sharp peak at the top end of the density of states at 514 cm^{-1}. This is associated with the interstitial and the neighboring atoms. The very highest-energy mode does not seem to be localized in nature, in contrast to the FFCD and split$\langle 110 \rangle$ defects.

The silicon vacancy shows several noticeable differences compared with the other defects. There is a substantial softening of phonons upon introduction of the defect. From Fig. 10, we see that the maximum phonon frequency at 501 cm^{-1} is significantly lower than the bulk value of 517 cm^{-1}. The last group of phonons in the bulk above 460 cm^{-1} has spread downwards to merge with the lower group of phonons. Using the LDA lattice constant of 5.387 Å we find that the acoustic phonons are unstable with one of the phonons having an imaginary frequency over much of the Brillouin zone. When the larger experimental lattice constant of 5.429 Å is used the acoustic phonons become stable. Such behavior is indicative of the extremely shallow nature of the energy surface associated with the vacancy. As a result of the unstable phonons the phonon density of states below

100 cm^{-1} does not have the same ω^2 dependence as the other defects and the bulk crystal. By making comparisons between results for the vacancy at both lattice constants we may ensure that this phonon instability does not alter our conclusions. Using this procedure we found that the substantial phonon softening observed for the vacancy is not an artifact caused by the instabilities but a real feature of the phonon spectrum for this defect. This softening plays an important role in the stabilization of the vacancy, as explored in the following section. The vacancy shows some resonant modes although there are no sharply defined peaks in the density of states as in the other defects. There is a mode at 118 cm^{-1} which consists mainly of motions of the four nearest neighbors of the vacancy which are shown in dark gray in Fig. 1. Each of these atoms has a displacement of 0.444. There is another mode at 67 cm^{-1} which is also centered on the four nearest neighbors of the vacancy. This is slightly less localized with the four atoms each having a displacement of 0.384.

VI. PHONON-FREE ENERGIES

The vibrational contribution to the free energy of a supercell containing N atoms within the harmonic approximation is

$$F_{vib} = 3Nk_BT \int_0^\infty \ln\left[2\sinh\frac{\hbar\omega}{2k_BT}\right] g(\omega)\, d\omega, \qquad (6)$$

where $g(\omega)$ is the phonon density of states normalized to unity. Inserting Eqs. (1) and (6) into Eq. (2) gives the vibrational contribution to the formation free energy of a defect. We have decided to separate the vibrational and static ground-state contributions because of the uncertainty which surrounds the latter due to the approximate treatment of electron correlation and the size of the simulation cell. It is likely that *ab initio* DFT methods give a good description of the vibrational spectra even though the treatment of electron correlation has a large effect on the formation energies, because the vibrational properties in the harmonic approximation are produced by infinitesimal displacements of the atomic positions that do not involve rebonding.

The vibrational contributions to the defect formation free energies for the various defects are shown as a function of temperature in Fig. 11. We see immediately that the effect of including phonons in the calculations is to lower the defect formation free energy at all temperatures. From Eq. (5) this lowering will lead to an increase in the concentration of all point defects. The zero-point energy of the phonons in the bulk is significantly larger than in the defective crystals, so that even at zero temperature the vibrational effects increase the concentration of defects. For the interstitial defects and FFCD this effect arises largely from the broadening of the high energy group of phonons between 460 and 500 cm^{-1} upon the introduction of the defects. From Figs. 6–8 we see that this broadening is asymmetric with most of the weight moving to lower frequencies just below 460 cm^{-1} where the group starts in the bulk. A smaller proportion moves to higher energies to form the sharp peaks near the bulk cutoff

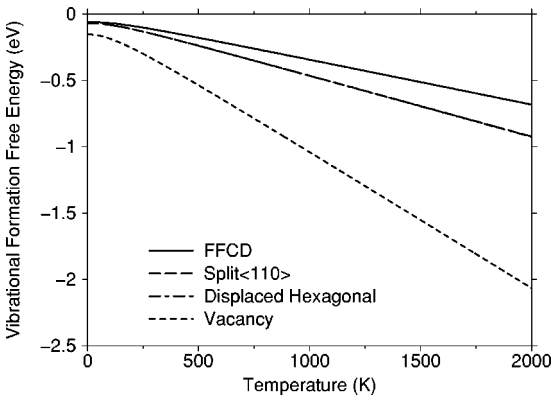

FIG. 11. Vibrational contribution to the defect formation free energy (the split⟨110⟩ and displaced hexagonal curves are indistinguishable).

which are associated with localized modes. The silicon vacancy has an even larger transfer of weight from high to low frequencies as can be seen from Fig. 10. The substantial softening of the high-frequency modes leads to a much smaller zero-point energy for the vacancy compared with the bulk crystal. The reduction in the formation free energy of the vacancy is much larger than for the other defects, especially at elevated temperatures, because of the phonon softening. By calculating the phonon spectrum of the FFCD in a 54-atom face-centered cubic supercell we have been able to estimate the error on the vibrational free energies of our defects. At 2000 K we estimate the error in the FFCD free energy to be about 0.15 eV. This error halves when moving to the lower temperature of 1000 K. This is smaller than the observed variations in formation energy seen in ground-state studies.

From Fig. 12 we see that as the temperature increases the difference between the vibrational energy of the defect and bulk crystals decreases. This is required by the law of Dulong and Petit which ensures in the high-temperature limit the difference vanishes as each mode of vibration contributes k_BT towards the total internal energy. The magnitude of the energy difference is always much smaller than the difference in vibrational formation free energies. This means that the

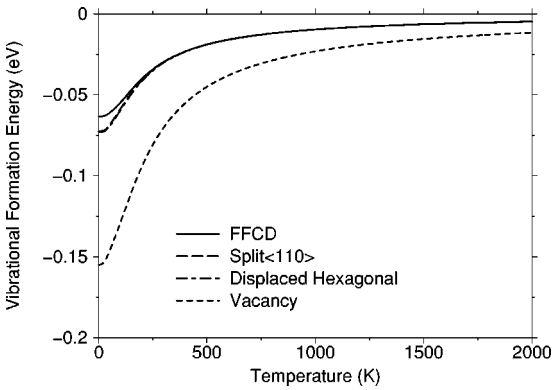

FIG. 12. Vibrational contribution to the defect formation energy (the split⟨110⟩ and displaced hexagonal curves are indistinguishable).

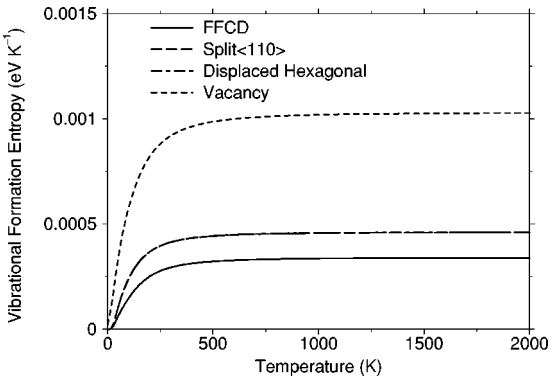

FIG. 13. Vibrational contribution to the defect formation entropy (the split$\langle 110\rangle$ and displaced hexagonal curves are indistinguishable).

continual decrease in defect formation free energy with increasing temperature observed in Fig. 11 must be due to the effects of the vibrational entropy. Figure 13 shows the vibrational formation entropy of the defects as a function of temperature. At very high temperatures the formation entropy converges to a positive constant value so that the formation free energy of the defects decreases linearly with temperature. The vibrational entropies of the defective crystals are greater than the entropy of the bulk solid. Such behavior has been observed for vacancies before.[28] We see that the vacancy has by far the largest formation entropy of the defects examined. This leads to the stabilization of vacancies with respect to the other defects as temperature is increased. At high temperatures the harmonic approximation that we have used is believed to break down due to an increase in the formation entropy[28] so that a fully anharmonic study is required. The primary effect of this is expected to be to further lower the defect formation free energies at higher temperatures.

Having obtained the vibrational contribution to the formation free energy of the defects we now calculate the total formation free energy of the defects and their associated equilibrium concentrations. Combining the results for the formation energies in Table I with the vibrational free energies given in Fig. 11 we obtain the total formation free energies shown in Fig. 14. We see immediately that the

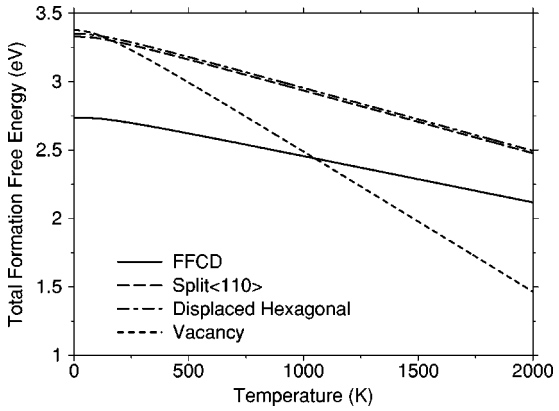

FIG. 14. Total defect formation free energies.

TABLE III. Number of degenerate configurations of the defects per atomic site.

	n_i
Vacancy	3
Hexagonal	2
Split$\langle 110\rangle$	6
FFCD	6
Displaced hexagonal	4

split$\langle 110\rangle$ and displaced hexagonal defects are not the most energetically stable at any temperature. At low temperatures the FFCD is the most stable and above 1049 K the vacancy becomes the most stable. The vacancy will always dominate at high temperatures because of the larger size of its formation entropy. The formation free energy for the vacancy is in broad agreement with the values obtained in a previous *ab initio* study[28] although the latter had a higher value which may be explained by uncertainties in the formation energy. The previous study[28] gave a zero-temperature formation energy of 4.1 eV for the vacancy which appears to be on the high side for a LDA-DFT calculation. This is most likely due to the smaller plane-wave cutoff and **k**-point grid used in that study. The calculated values for the formation entropy are similar although our study produces a higher value which is important for stabilization of the vacancy at high temperatures. Both *ab initio* studies give estimates of the change in free energy with temperature which are very much larger than those obtained in earlier empirical potential calculations.[25]

We now use the total formation free energies together with the numbers of degenerate configurations for each defect listed in Table III to calculate the intrinsic equilibrium concentrations from Eq. (5), taking $n_s = 5.1\times 10^{22}$ cm^{-3}. We plot the equilibrium concentrations against inverse temperature in Fig. 15. We see that the concentrations of vacancies and FFCDs are equal at a temperature of 1150 K, with the vacancies predominating at higher temperatures and the FFCD defects at lower ones. Eaglesham[5] gives a rough experimental estimate of the concentrations of interstitials and vacancies at 1073 K of 5×10^{10} cm^{-3}. At this temperature

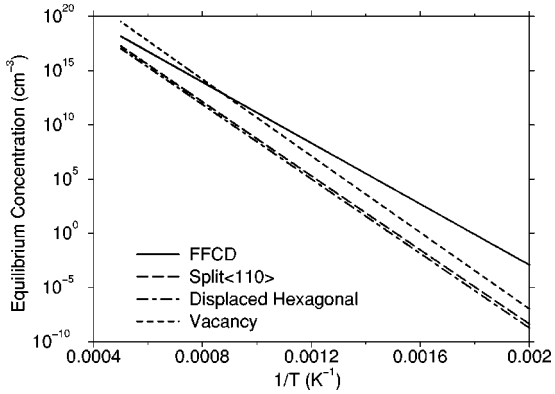

FIG. 15. Equilibrium defect concentrations as a function of inverse temperature.

our estimates for the split$\langle 110 \rangle$ and displaced hexagonal defects are approximately 10^{10} cm^{-3} which agrees quite well with experiment. For the vacancy we have a higher concentration of 10^{12} cm^{-3} which is greater than the experimental value but is still consistent given the experimental uncertainties. Fahey *et al.*[29] give experimental estimates of the defect concentration at the higher temperatures in the region of 1500 K for both interstitials and vacancies. Their results give concentrations of about 10^{14} cm^{-3} for interstitials and 10^{14}–10^{16} cm^{-3} for vacancies. The split$\langle 110 \rangle$ and displaced hexagonal defects again agree with the interstitial value at approximately 10^{14} cm^{-3}. The FFCD has a slightly higher concentration at 10^{15} cm^{-3}. The vacancy comes in at the top of the range of estimated values at a concentration of 10^{16} cm^{-3}. Overall our results are broadly consistent with the available experimental estimates[5,29] which, however, vary greatly.

The present study has ignored the effects of electronic excitations which also contribute to the free energy of solids. The greatest contribution is expected to occur for the silicon vacancy which has defect states within the band gap. This leads to a contribution to the formation entropy which has been estimated[28] to be about 1–2 k_B or approximately 10% of the vibrational contribution. This will further increase the concentration of vacancies at high temperatures.

VII. CONCLUSIONS

At high temperatures the vibrational free energy associated with a point defect in silicon is of order 1 eV, which is a substantial contribution given that typical formation energies are a few eV. This stabilization is especially large for the vacancy which, because of its large formation entropy, is predicted to predominate at high temperatures. At the temperature range of 1000–1100 K where silicon devices are thermally processed we see that both interstitials and vacancies exist in roughly equal measure which agrees with current opinion. The FFCD is more stable than both the split$\langle 110 \rangle$ and displaced hexagonal defects up to very high temperatures, because of its lower formation energy. The hexagonal defect is unstable with respect to a small displacement of the interstitial atom which lowers the formation energy. The phonon spectra of the defective crystals exhibit localized vibrational modes.

ACKNOWLEDGMENTS

Financial support was provided by the Engineering and Physical Sciences Research Council (EPSRC), UK. Computational facilities were provided by the High Performance Computing Facility at the University of Cambridge, and the Computer Services for Academic Research (CSAR) in Manchester, UK.

*Electronic address: oka20@phy.cam.ac.uk

[1] G. D. Watkins, *Defects and Their Structure in Non-metallic Solids* (Plenum, New York, 1976), p. 203.
[2] S. Dannefaer, P. Mascher, and D. Kerr, Phys. Rev. Lett. **56**, 2195 (1986).
[3] U. Gösele, A. Plössl, and T. Y. Tan, *Process Physics and Modeling in Semiconductor Technology* (Electrochemical Society, Pennington, New Jersey, 1996), p. 309.
[4] H. Bracht, E.E. Haller, and R. Clark-Phelps, Phys. Rev. Lett. **81**, 393 (1998).
[5] D. Eaglesham, Phys. World **8**, 41 (1995).
[6] S. Goedecker, T. Deutsch, and L. Billard, Phys. Rev. Lett. **88**, 235501 (2002).
[7] J.P. Perdew and Y. Wang, Phys. Rev. B **45**, 13 244 (1992).
[8] S. Baroni, S. de Gironcoli, A.D. Corso, and P. Giannozzi, Rev. Mod. Phys. **73**, 515 (2001).
[9] The ABINIT code is a common project of the Université Catholique de Louvain, Corning Incorporated, and other contributors (URL http://www.abinit.org).
[10] N. Troullier and J.L. Martins, Phys. Rev. B **43**, 1993 (1991).
[11] H.J. Monkhorst and J.D. Pack, Phys. Rev. B **13**, 5188 (1976).
[12] R.P. Feynman, Phys. Rev. **56**, 340 (1939).
[13] M.I.J. Probert and M.C. Payne, Phys. Rev. B **67**, 075204 (2003).
[14] M.J. Puska, S. Pöykkö, M. Pesola, and R.M. Nieminen, Phys. Rev. B **58**, 1318 (1998).
[15] M. Tang, L. Colombo, J. Zhu, and T.D. de la Rubia, Phys. Rev. B **55**, 14 279 (1997).
[16] F. Cargnoni, C. Gatti, and L. Colombo, Phys. Rev. B **57**, 170 (1998).
[17] R.J. Needs, J. Phys.: Condens. Matter **11**, 10 437 (1999).
[18] W.-C. Lee, S.-G. Lee, and K.J. Chang, J. Phys.: Condens. Matter **10**, 995 (1998).
[19] J. Zhu, L.H. Yang, C. Mailhiot, T.D. de la Rubia, and G.H. Gilmer, Nucl. Instrum. Methods Phys. Res. B **102**, 29 (1995).
[20] W.-K. Leung, R.J. Needs, G. Rajagopal, S. Itoh, and S. Ihara, Phys. Rev. Lett. **83**, 2351 (1999).
[21] W.M.C. Foulkes, L. Mitas, R.J. Needs, and G. Rajagopal, Rev. Mod. Phys. **73**, 33 (2001).
[22] SCHAKAL 99. A computer program for the graphic representation of molecular and crystallographic models.
[23] J.L. Mercer, J.S. Nelson, A.F. Wright, and E.B. Stechel, Modell. Simul. Mater. Sci. Eng. **6**, 1 (1998).
[24] A. Antonelli, E. Kaxiras, and D.J. Chadi, Phys. Rev. Lett. **81**, 2088 (1998).
[25] S.J. Clark and G.J. Ackland, Phys. Rev. B **48**, 10 899 (1993).
[26] S.J. Clark and G.J. Ackland, Phys. Rev. B **56**, 47 (1997).
[27] G. Dolling, *Inelastic Scattering of Neutrons in Solids and Liquids* (IAEA, Vienna, 1963), Vol. II, p. 37.
[28] R. Car, P.E. Blöchl, and E. Smargiassi, Mater. Sci. Forum **83–87**, 443 (1992).
[29] P.M. Fahey, P.B. Griffin, and J.D. Plummer, Rev. Mod. Phys. **61**, 289 (1989).